Long-range phase synchronization of high-gamma activity in human cortex

Arnulfo G[1,4,†,*], Wang SH[1,2,3,†], Williams N[1], Hirvonen J[1,2], Fato MM[4], Nobili L[5,6], Cardinale F[5], Rubino A[5], Zhigalov A[1], Palva S[1,3,7], Palva JM[1,7,*]

[1] *Neuroscience Center, Helsinki Institute of Life Science, University of Helsinki, Finland*

[2] *Doctoral Programme Brain & Mind, University of Helsinki, Finland*

[3] *BioMag laboratory, HUS Medical Imaging Center, Helsinki, Finland*

[4] *Dept. of Informatics, Bioengineering, Robotics and System engineering, University of Genoa, Genoa, Italy*

[5] *"Claudio Munari" Epilepsy Surgery Centre, Niguarda Hospital, Italy*

[6] *Child Neuropychiatry, G. Gaslini Institute, DINOGMI, University of Genoa, Genoa, Italy*

[7] *Center for Cognitive Neuroimaging, Institute of Neuroscience and Psychology, University of Glasgow, United Kingdom*

[†] *These authors contributed equally*

[*] *Correspondence should be addressed to:*

Gabriele Arnulfo

gabriele.arnulfo@dibris.unige.it

and/or to:

J. Matias Palva

matias.palva@helsinki.fi

Running Title: Cortical architecture of high-gamma phase synchronization

Number of Pages: 11

Number of words in main text:3841/4500

Number of Figures and tables: 8/8

Number of words in the abstract: 146/100-150

Number or words in the introduction: 537

Number of words in the discussion: 1351

Data Availability: Raw data and patient details cannot be shared due to Italian governing laws as well as Ethical committee restrictions. Intermediate as well as final processed data that support the findings of this study are available from the corresponding author upon reasonable request.

Author contributions: AG WSH PJM PS conceived the study; AG WSH WN ZA PJM wrote the analysis code; AG WSH WN HJ run the analysis; CF NL RA provided clinical information and preprocessed clinical data. All authors contributed to the writing and revising the manuscript. All authors read and approved the manuscript.

Abstract

Inter-areal neuronal phase synchronization is thought to involve oscillations below 100 Hz while faster oscillations are presumed to be coherent only in local circuits. We show with human intracerebral recordings that 100−300 Hz high-gamma activity (HGA) can be phase synchronized between widely distributed regions. HGA synchronization was neither attributable to physiological and technical artefacts nor to epileptic pathophysiology, *e.g.*, it was as prevalent in areas distant from the epileptic zone as within. HGA phase synchronization exhibited a reliable large-scale connectivity and cortex-wide community structures. Moreover, HGA synchronization displayed a laminar profile opposite to that of low-frequency oscillations by being stronger between the deep than the superficial cortical layers. Hence HGA synchronization constitutes a novel and temporally highly accurate form of consistent timing relationships in large-scale human cortical activity. We suggest that HGA synchronization elucidates the temporal microstructure of spiking-based neuronal communication *per se* in cortical circuits.

Keywords: ripple, high gamma activity, high-frequency oscillations, synchronization, functional connectivity, epilepsy

Abbreviations:
cPLV: complex-valued phase-locking-value (Methods eq.1)
EZ: epileptogenic zone
HFO: high-frequency oscillations (100−200 Hz)
HGA: high-gamma activity (100−300 Hz)
iPLV: the imaginary part of the complex PLV
LFP: local-field potential
nEZ: putative healthy SEEG recording sites
PLV: the absolute value of the complex PLV
SEEG: stereo-electroencephalography

Introduction

Observations of organized neuronal population activities at frequencies above 100 Hz, such as high-gamma activity (HGA, 100−300 Hz)[1], high-frequency oscillations (HFOs, 100−200 Hz) and ripple oscillations (150–200 Hz)[2,3] are abundant in electrophysiological recordings from cortical structures of humans[1,4] and experimental animals[5,6]. Several lines of evidence link HGA with perceptual and cognitive processes[1,4,7–9], and overall indicate that high-amplitude HGA is a key signature of "active" neuronal processing. Ripple oscillations have been traditionally associated with sharp waves and off-task memory formation, but recent studies report ripples also during the performance of attention tasks[10]. Occasionally HGA and HGOs are referred to as ripple oscillations in human intra-cranial recordings. In this study, we refer HGA to oscillatory activity between 100−300 Hz.

Electrophysiological HGA signals are thought to mainly arise from broad-band multi-unit spiking activity (MUA) and hence to directly reflect the local peri-electrode neuronal population activity *per se*[11,12]. HGA[13] and ripple oscillation signals do, however, also contain contributions from post-synaptic potentials. While the synaptic mechanisms underlying the hippocampal ripple oscillations are already well understood, it appears that genuine oscillations with presumably synaptic-communication-based mechanisms also contribute to the HGA signals[13].

HGA has been thought to be exclusively local in terms of spike synchronization and phase coupling. For slower (< 100 Hz) neuronal oscillations, phase relationships among distributed neuronal assemblies are instrumental for coordinating neuronal communication and processing[14,15]. Several lines of experimental and theoretical evidence have shown that these phase relations are dependent on frequency and neuroanatomical distance, and on the axonal conduction delays in particular, so that slow oscillations are generally more readily phase coupled over long distances than fast oscillations[16–18]. In line with this notion, measurements of long-range phase coupling in animal[15,19] and human[16] brains suggest that neuronal oscillations only in frequency bands below 100 Hz exhibit inter-areal phase synchronization[20] whereas the inter-areal cooperative mechanisms of HGA have remained poorly understood.

We hypothesized that long-range synchronization and phase coupling of HGA could nevertheless be conceivable because local synchronization and high collective firing rate can endow local pyramidal cell populations greatly enhanced efficiency in engaging their post-synaptic targets[21], which would be experimentally observable as inter-areal HGA phase coupling. Such a finding would constitute a direct observation of the actual spiking-based long-range neuronal

communication *per se*. Nevertheless, there is little evidence for HGA synchronization over long distances so far[22].

In this study, we searched for long-range HGA synchronization using an extensive database of resting-state human stereo-electroencephalography (SEEG) recordings ($N = 67$). We used sub-millimeter accurate SEEG-electrode localization[23] and white-matter referencing[16] to obtain neocortical local-field potential (LFP) signals with little distortion from signal mixing with neighboring grey-matter or distant volume-conducted sources. We found that among these LFPs, long-range HGA synchronization was a surprisingly robust phenomenon and much stronger than synchronization at around 100 Hz. We rigorously excluded the possibilities of HGA synchronization being attributable to putative confounders such as the epileptiform pathophysiology or physiological and technical artefacts. The network architecture of resting-state functional connectivity achieved by HGA synchronization was split-cohort reliable and had a modular large-scale architecture that were distinct from those of lower frequencies. These findings thus reveal in the human brains a novel form of spatio-temporally highly accurate neuronal coupling and thereby elucidate the cerebral organization of fast neuronal communication.

Results

Probing human large-scale brain dynamics with SEEG

We recorded ~10 minute resting-state human cortical (local-field potential) LFP signals from 92 consecutive patients with stereo-electroencephalography (SEEG). Among them, 25 subjects were excluded from further analyses due to previous brain surgery (temporal lobotomy) or an MRI-identified cortical malformation (Table 1, Suppl. Fig. 1). The final cohort of 67 patients yielded a total of 7068 non-epileptic grey matter contacts (113 ± 16.2 per subject, mean $\pm$ SD, range 70-152) that gave a dense sampling across all neocortical regions (Fig. 1a) and of seven canonical functional brain systems defined by fMRI intrinsic connectivity mapping[24,25] (Fig. 1b).

We assessed the phase interactions between all LFP signals recorded from non-epileptic neocortical grey-matter locations. This yielded a dense coverage of cortical interactions with $5,493 \pm 1,627$ (mean $\pm$ SD) contact pairs per subject (range: 2,094–9,947) and a total of 368,043 contact pairs. Out of all possible within-hemispheric connections in the 100-parcel Schaefer atlas[25], these recordings sampled at least 80% of the left- and 90% of the right-hemispheric connections (Fig. 1c) and provided abundant sampling on the scale of functional systems (Fig. 1d). The present data thus yield comprehensive insight into large-scale dynamics and connectivity in human brains.

4

Long-range phase correlations in high-gamma activity

We estimated inter-electrode-contact phase coupling with the phase-locking value (PLV) for 18 frequency bands between 3 and 320 Hz (see Methods). The inter-contact PLV estimates were averaged across subjects for three inter-contact-distance ranges quartiles for each frequency band (Fig. 2a). The first quartile (0−2 cm), was excluded to avoid contamination of residual effects of volume conduction. We found that the mean PLV increased from 3 to 7 Hz and then decayed rapidly from 100 Hz as expected[16]. However, from 100 Hz onward, the mean PLV increased monotonically, indicating highly significant HGA phase synchronization in all distance ranges.

To quantify the neuro-anatomical extent of HGA synchronization, we assessed the connection density, K, that was defined as the fraction of contact pairs exhibiting significant ($p <$ 0.001 for observed > surrogate PLV) phase synchronization (Fig. 2b). Even at long ranges (> 6 cm), more than 70% of >100 Hz connections were significant and both the PLV and K findings were split-cohort reliable (Suppl. Fig. 5). HGA phase synchronization was thus a widespread phenomenon in SEEG recordings of resting-state brain activity.

Visual inspection of HGA synchronization in SEEG electrode time series (Fig. 2 c−f) was in line with these observations and readily revealed episodes of significant HGA coupling in time windows across centimeter-scale distances. Notably, synchronized HGA was observed as low-amplitude oscillation-like activity that was visible in the time series also without filtering, which provides first evidence for that it is not attributable to spikes or technical artefacts.

Given the novelty and unexpected nature of these observations, we performed extra sets of control analyses to exclude the possibilities that the observed large-scale HGA synchronization were due to: referencing schemes and volume conduction (Suppl. Fig. 2 & 3), non-neuronal signal sources (Suppl. Fig. 4), inadequate filter attenuation or settings (Suppl. Fig. 6), amplifier noise or pathological neuronal activity, such as inter-ictal spikes, or contamination from muscular signals (Suppl. Fig. 7). The results of these analyses converged on the conclusion that the seemingly anomalous HGA synchronization can only be explained by true long-range synchronization between local cortical neuronal assemblies (Suppl. Text). This conclusion was further consolidated by the findings, as detailed below, that HGA synchronization was predominant in specific functional systems, and had a community structure and laminar connectivity profile that were distinct from those of slower activities, which are inconceivable for technical or physiological artefacts.

Neuroanatomical localization of high-gamma synchronization

To characterize the neuro-anatomical features of HGA synchronization networks, we investigated large-scale phase coupling of HGA in two spatial resolutions. First on the level of functional systems[24], robust HGA phase synchrony was found within and between all systems, but the strongest and most widespread phase synchrony was found between and within the default-mode (DEF) and limbic (LIM) systems (Fig. 3a,b). This observation is in line with the hypothesis that HGA synchronization reflects healthy patterns of neuronal communication that is dominated by activity in these systems, DEF in particular[26], during resting state. The observed systems-level connectivity pattern was split-cohort reliable (Suppl. Fig. 5), which rules out biases of individual subsets with distinct aetiologies.

To examine the architecture of HGA synchronization at a finer resolution, we used the 100-parcel Schaefer atlas[25] and pooled data across subjects to estimate the connectome of inter-regional phase-synchrony for each frequency. We found these connectomes to be split-cohort reliable (permutation test, $p < 0.05$, N=1000, one-tailed) across the range of frequency bands investigated, including the HGA frequency band (Suppl. Fig. 5).

We then applied Louvain community detection to identify the putative communities therein and found sets of regions to represent robust modules in the HGA frequency bands (see Suppl. Text). The numbers of regions assigned reliably to communities were much higher than expected by chance (bootstrapping test, $p < 0.05$, N=100, one-tailed) for each HGA frequency and throughout the investigated range of the Louvain resolution parameter γ (1−1.5) (Suppl. Fig. 10), i.e. the parameter influencing the number of communities returned. Most of these networks also demonstrated significant community structures compared to equivalent random networks (permutation test, $p < 0.05$, N=100, one-tailed) at a range of resolutions (Suppl. Fig. 10).

For the connectome at 190 Hz, majority of the communities (Fig. 3c) comprised adjacent brain regions but also included some spatially distant regions. The existence of spatially distant regions within the same community is a clear demonstration of strong phase-coupling between such regions (Fig. 3d). For the 190 Hz connectome, at a low spatial resolution, the network was split into four large communities which became divided into smaller ones at higher resolutions resulting in six to seven communities (Fig. 3d). The whole-brain networks of HGA synchronization thus exhibited statistically significant community structures in putatively healthy brain structures, as well as patterns of connection strengths that are stable across participants. These results further support the neurobiological origin of HGA synchronization.

High-gamma phase correlations have a unique laminar profile

Deep and superficial cortical laminae are known to contribute differently to inter-areal phase-synchronization at frequencies below 100 Hz[16]. We next asked whether HGA synchronization networks also would show a similar differentiation between the laminae across distances. Leveraging our accurate localization of the electrode contacts, we divided the electrode contacts into "deep" and "superficial" by their cortical depth (see Methods), and assessed HGA phase coupling strength separately between the contacts in deep and superficial layers. This analysis reproduced our prior observation[16] of low-frequency (< 30 Hz) phase coupling being predominantly observed among superficial sources, which is well in line with recent observations about the laminar localization of, *e.g.*, alpha oscillation sources in human cortex[27]. In contrast, however, HGA synchronization was stronger (Fig. 4a, see inset) and more prevalent (Fig. 4b) among signals from deep cortical layers in all distance ranges (100 permutations, $p < 0.05$, Bonferroni corrected with $N_{freq.} = 18$). This reverse pattern was also observed with iPLV and in bipolar recordings (Suppl. Fig. 3). Although the resolution of SEEG is insufficient for further investigating the underlying neuronal generators of these oscillations, *e.g.*, with a current source density analysis, our results indicate that HGA synchronization originates in neuronal circuitry distinct from that producing the slower LFP oscillations.

Long-range HGA synchronization is associated with local synchronization indexed by HGA amplitude

To further delve into the physiological plausibility of HGA synchronization, we asked whether it was related to the moment-to-moment variability in the amplitudes of local HGA. HGA amplitude is likely to tightly reflect the number of neurons in the local assembly and the degree of their local synchronization, both of which are central to the ability of a local assembly to engage its post-synaptic targets effectively. We thus hypothesize that the moments of strongest inter-areal HGA phase synchrony would coincide with the moments when both contacts recorded high HGA amplitudes. We selected electrode contacts exhibiting significant HGA synchronization and for each contact pair, distributed the data sample-by-sample into a 2D matrix according to quintiles of the normalized local amplitudes (see Methods). First, inspecting the variability in the numbers of samples among the cells of these 2D matrices we found that there was a slight positive correlation between the amplitudes so that the coincidence of the largest-quintile amplitudes was ~1 % more prevalent than the coincidence of the smallest and largest amplitudes. Second, after equalizing the sample counts in amplitude quintile pairs, we estimated the PLV from samples in each quintile pair, and averaged the PLVs across electrode pairs and subjects. We found that while HGA phase

coupling was significant across a range of local amplitudes, it was the strongest in those moments when the HGA amplitudes were the largest in both contacts and essentially insignificant when either location exhibited the lowest HGA amplitudes (Fig. 5a, b). Quantitatively, PLV was very dependent on the local oscillation amplitudes and exhibited a ~400 % difference between smallest and largest values in data averaged across the HGA band and a 200-800% difference in individual HGA frequencies with the strongest effects observed at highest frequencies (Suppl. Fig. 9). These data thus strongly support the notion of local HGA synchronization being instrumental for long-range HGA phase coupling.

Phase-amplitude coupling (PAC) of HGA with theta and alpha oscillations characterizes healthy brain dynamics

The "nesting" of fast oscillations in cycles of slower oscillations is an often-observed phenomenon in electrophysiological recordings at both < 1 Hz[28,29] and > 1Hz frequencies. We assessed whether HGA were nested within specific phase of slow rhythms by evaluating phase-amplitude correlations (see Methods) throughout the 3−320 Hz frequency range and among all pairs, excluding self-connections, of grey matter electrode contacts. We analyzed data from electrode contacts in the epileptogenic zone (EZ) to dissociate healthy from pathological patterns of PAC.

Among the putatively healthy LFP recordings, *i.e.*, nEZ contacts, the amplitudes of beta and low-gamma oscillations (14−40 Hz) were strongly coupled with the phase of theta and alpha oscillations (5−10 Hz) (Fig. 6a). Importantly, the amplitudes of HGA, peaking between 100−200 Hz, exhibited clear coupling with the phase of these theta−alpha oscillations. However, a fundamentally distinct cross-frequency PAC pattern was observed within the EZ (Fig. 6b), where instead of predominant narrow-band theta/alpha coupling, the amplitudes of oscillations from the lowest frequencies to HGA were locked to the phase of delta-band (here 3 Hz) oscillations. This putatively pathological pattern was also reflected in PAC evaluated between the healthy and epileptic areas, which exhibited both the delta and theta/alpha nesting of faster activities (Fig. 6c).

Is high-gamma synchrony a feature of epileptic brain tissue?

A crucial question for the functional implications of HGA synchronization is whether it is mainly a pathological property of the epileptogenic network or a feature of healthy brain activity and neuronal communication therein. The earlier finding of systematic HGA community structures across subjects with diverse aetiologies already provided evidence in support of the latter alternative. We further addressed this question first by asking whether the strength of HGA synchronization was significantly stronger in the EZ or between the EZ and nEZ. Controlling for

8

the neuroanatomical distance of the electrode-electrode interactions, we found the epileptogenic zone to exhibit significantly stronger phase synchronization than healthy areas at low frequencies (3−10 Hz) but no significant differences were observed in the HGA frequency band (Fig. 7, see also Suppl. Fig. 7e).

We then tested whether the strength of HGA synchronization overall was correlated with the frequency of inter-ictal spikes; a proxy for the magnitude of epileptic pathology. No such correlation was observed (Suppl. Fig. 7c). These data thus converged onto the conclusion that HGA synchronization is a property of healthy brain dynamics that is preserved in these patients.

Discussion

Strong correlation of HGA with neuronal firing rate and the BOLD signal[30,31], as well as the ubiquitous association of cortical HGA with a range of cognitive processes[1,4,7–9] have led to the notion of HGA being a direct indication of 'active' neuronal processing *per se*[1,4–6]. In the same frequency range, high-frequency oscillations (HFOs) are predominantly observed in epileptogenic brain areas and are elevated in magnitude prior to epileptic seizures[32]. The relationship between HGA and HGOs has remained unclear; HFOs may either be a phenomenon separate from HGA and integral to epileptic pathophysiology or, alternatively, pathological modulation of otherwise physiological HGA that also is known to exhibit oscillatory temporal patterning[13].

In either case, little is known about the large-scale phase synchrony of HGAs or HFOs, and they have been considered exclusively as local phenomena. HGA *amplitude* fluctuations may be coupled inter-areally in human cortical networks during reading[33], and similarly, ripple oscillations bursts co-occur between the rat hippocampus and association cortices during memory formation[34]. However, amplitude correlation does not have the temporal precision that phase-coupling has for carrying out important computational functions during neuronal processing. Nonetheless, inter-areal phase-coupling has been thought to exist only in slow brain rhythms but not in HGA frequency bands. To the best of our knowledge, there is only one reported HGA inter-areal *phase* coupling[22]. In this study, Yamamoto et al (2014) reported phase synchronization of ripple oscillations within the entorhinal-hippocampal circuit in behaving rats.

We report here that in the human brains, neuronal activity in the 100−300 Hz frequency range may be phase synchronized across several centimeters during awake resting-state brain activity. Long-range synchronization was highly reliable and not explained by physiological or technical artefacts in the recorded data. HGA synchronization was also primarily a physiological phenomenon and not

9

explained by epileptic pathophysiology. HGA synchronization thus constitutes a novel form of neuronal long-range coupling in the dynamic functional architecture on human brain dynamics. We suggest that these observations of HGA synchronization open a new avenue into measuring and understanding neuronal communication in the human brains at the level of pre-synaptic population spiking, spike synchronization, and their post-synaptic potentials in remote targets.

Micro- and macroscale cortical architecture of HGA synchronization

HGA synchronization exhibited systematic organization at several spatial and temporal scales. At the level of cortical systems determined by fMRI intrinsic connectivity[24], HGA synchronization was most pronounced within and between the limbic- and default-mode systems. These areas exhibit high level of activity during resting-state [26] and thus this finding is in line with the notion that HGA synchronization reflects neuronal processing or communication *per se*. Interestingly, in a subset of subjects who had recordings both during resting-state and during sleep, we found differences in HGA synchronization patterns between these two conditions (Suppl. Fig. 8). This suggests that HGA synchronization is state-dependent similar to fMRI resting-state connectivity in humans [35] and non-human primates[36].

In addition to this insight into HGA synchronization among fMRI-derived brain systems, we examined the intrinsic community structure in the whole-brain connectome of HGA synchronization. We found evidence for significant and split-cohort reliable community structures in HGA synchronization. Together with the split-cohort reliability of the connectome itself, these findings show that HGA synchronization has a group-level stable cortical topology that is independent of individual subjects and thus also a structure that is not dictated by the individual pathogenesis or electrode placement. Moreover, this ties HGA synchronization with phase and amplitude interaction networks in slower frequencies, which as known to have salient community structures[37–40]. The HGA communities, however, were dissimilar with those at slower frequencies, which may be attributable to distinct cortical generator mechanisms of the slow and HGA signals. This conclusion was supported by the finding that at the scale of cortical laminae, HGA synchronization was significantly stronger among electrode contacts in deep than superficial layers whilst the opposite laminar organization was found for theta, alpha, and beta oscillations in SEEG here and in prior work[16]. HGA synchronization thus exhibits reliable neuroanatomical organization at scales from cortical laminae to brain systems with phenomenological differences with the oscillations in slower frequencies. HGA synchronization is thus not a "by-product" of neuronal interactions coupling the slower oscillations, but rather a hitherto undiscovered component in the organization of large-scale brain dynamics.

10

HGA synchronization is not attributable to artefactual sources

The connectivity and community structures of HGA synchronization as well as its laminar organization strongly suggest that it may not be attributable to physiological or technical artefacts such as signals from muscles or extra-cranial sources. Nonetheless, we corroborated this notion with a number of controls. First, in addition to white-matter referencing, HGA synchronization was observable with bipolar referencing, indicating that its current sources are millimeter-scale local in cortical tissue and very unlikely to originate from extracranial or muscular sources during inter-ictal events[41]. Second, HGA synchronization was also observable with linear-mixing insensitive interactions metric and hence not attributable to volume conduction[42]. Third, HGA synchronization was comparable among electrodes along single electrode shafts and between electrodes in different shafts, which excludes the contributions of implantation-related lesion along the shafts as well as voltage diffusion because of perfusion of CSF in the cortical lesion following shafts implant. Fourth, similar observations were made with two different SEEG data-acquisition systems and the recordings with the same electrodes in saline solution did not show any indication of artificial HGA synchronization. HGA coupling thus does not arise from the signal amplifier or data-acquisition electronics.

HGA activity is not explained by pathological epileptic activity

The role of epileptic pathology is overall a concern for research carried out with epileptic patients. Although HGA within the epileptogenic zone show peculiar spectral and amplitude contents[43,44], and are temporally predictive of upcoming seizures, most recent work has questioned its pathological-only origin[45,46]. We addressed question of physiological vs. pathophysiological genesis of HGA synchronization through several lines of analyses. First, only the putatively healthy brain areas and time-windows with no epileptic spikes were included in the primary analyses of HGA synchronization. Second, if HGA synchronization was attributable to epileptic pathophysiology, one would expect highly individual large-scale patterns, but instead of such, we observed that both the connectivity and community structures of HGA were split-cohort reliable at the group level and thus not driven by individual pathology. Third, in direct comparisons of HGA synchronization among healthy areas, between healthy areas and the epileptic zone, and within the epileptic zone, we did not find significant differences between these conditions. We found the epileptic zone to be distinct from healthy brain areas both in delta-frequency phase synchronization and in the phase-amplitude coupling of delta and theta oscillations with HGA. Hence, if HGA synchronization were a property of the epileptic zone, it would likely have been observed in this analysis. Finally, we observed no phase coupling of HGA with epileptic spikes. Taken together, HGA synchronization

11

appears to be a property of healthy brain dynamics rather than being attributable to epileptic activity or pathophysiology.

Putative generative mechanisms HGA synchronization

What mechanisms could underlie the signal generation of long-range phase coupled HGA? Whereas synaptic mechanisms are known to contribute to the generation of synchronized ~200 Hz oscillations during hippocampal sharp-wave events[47], it has remained disputed whether broad-band HGA in the 100-300 Hz range is associated with synaptic mechanisms generating neuronal population oscillations with rhythmicity in specific time scales[19]. A recent study[13] argues that putetively-spiking-related broadband and genuinely oscillatory components with presumably synaptic-communication-based mechanisms are dissociable in the HGA signals, even though several studies suggest HGA to arise from neuronal spiking activity[48,49] *per se*. We speculate that the HGA signals observed in this study may reflect both local cortical population spiking activity and the consequent downstream post-synaptic potentials resulting from these volleys of spikes. Long-range MUA synchronization has not been previously reported, but it is important to note that unlike the micro-electrodes used in animal research, the larger surface area of the electrodes heavily predisposes SEEG specifically to detecting population spiking activity[50] that is already locally synchronized in a sizeable assembly and thus able to achieve post-synaptic impact in distant targets[21]. Hence, by construction, SEEG may be effectively filtering out asynchronous multi-unit activity that is unlikely to achieve well-timed downstream effects.

References

1. Lachaux, J. P., Axmacher, N., Mormann, F., Halgren, E. & Crone, N. E. High-frequency neural activity and human cognition: Past, present and possible future of intracranial EEG research. *Progress in Neurobiology* (2012). doi:10.1016/j.pneurobio.2012.06.008

2. Logothetis, N. K. *et al.* Hippocampal-cortical interaction during periods of subcortical silence. *Nature* (2012). doi:10.1038/nature11618

3. Novitskaya, Y., Sara, S. J., Logothetis, N. K. & Eschenko, O. Ripple-triggered stimulation of the locus coeruleus during post-learning sleep disrupts ripple/spindle coupling and impairs memory consolidation. *Learn. Mem.* (2016). doi:10.1101/lm.040923.115

4. Parvizi, J. & Kastner, S. Promises and limitations of human intracranial electroencephalography. *Nature Neuroscience* (2018). doi:10.1038/s41593-018-0108-2

5. Buzsáki, G. & Silva, F. L. da. High frequency oscillations in the intact brain. *Progress in Neurobiology* (2012). doi:10.1016/j.pneurobio.2012.02.004

6. Engel, J. & da Silva, F. L. High-frequency oscillations - Where we are and where we need to

go. *Progress in Neurobiology* (2012). doi:10.1016/j.pneurobio.2012.02.001

7. Ray, S., Niebur, E., Hsiao, S. S., Sinai, A. & Crone, N. E. High-frequency gamma activity (80-150 Hz) is increased in human cortex during selective attention. *Clin. Neurophysiol.* (2008). doi:10.1016/j.clinph.2007.09.136

8. Haller, M. *et al.* Persistent neuronal activity in human prefrontal cortex links perception and action. *Nat. Hum. Behav.* (2018). doi:10.1038/s41562-017-0267-2

9. Sellers, K. K. *et al.* Oscillatory Dynamics in the Frontoparietal Attention Network during Sustained Attention in the Ferret. *Cell Rep.* (2016). doi:10.1016/j.celrep.2016.08.055

10. Johnson, E. L. & Knight, R. T. Intracranial recordings and human memory. *Current Opinion in Neurobiology* (2015). doi:10.1016/j.conb.2014.07.021

11. Ray, S., Hsiao, S. S., Crone, N. E., Franaszczuk, P. J. & Niebur, E. Effect of Stimulus Intensity on the Spike-Local Field Potential Relationship in the Secondary Somatosensory Cortex. *J. Neurosci.* (2008). doi:10.1523/JNEUROSCI.1588-08.2008

12. Ray, S. & Maunsell, J. H. R. Different origins of gamma rhythm and high-gamma activity in macaque visual cortex. *PLoS Biol.* (2011). doi:10.1371/journal.pbio.1000610

13. Scheffer-Teixeira, R., Belchior, H., Leao, R. N., Ribeiro, S. & Tort, A. B. L. On High-Frequency Field Oscillations (~100 Hz) and the Spectral Leakage of Spiking Activity. *J. Neurosci.* (2013). doi:10.1523/JNEUROSCI.4217-12.2013

14. Bastos, A. M., Vezoli, J. & Fries, P. Communication through coherence with inter-areal delays. *Curr. Opin. Neurobiol.* **31,** 173–180 (2015).

15. Buzsáki, G. & Schomburg, E. W. What does gamma coherence tell us about inter-regional neural communication? *Nature Neuroscience* (2015). doi:10.1038/nn.3952

16. Arnulfo, G., Hirvonen, J., Nobili, L., Palva, S. & Palva, J. M. Phase and amplitude correlations in resting-state activity in human stereotactical EEG recordings. *Neuroimage* (2015). doi:10.1016/j.neuroimage.2015.02.031

17. Leopold, D. A., Murayama, Y. & Logothetis, N. K. Very Slow Activity Fluctuations in Monkey Visual Cortex: Implications for Functional Brain Imaging. *Cereb. Cortex* **13,** 422–433 (2003).

18. Von Stein, A. & Sarnthein, J. Different frequencies for different scales of cortical integration: From local gamma to long range alpha/theta synchronization. in *International Journal of Psychophysiology* (2000). doi:10.1016/S0167-8760(00)00172-0

19. Buzsáki, G. & Wang, X.-J. Mechanisms of Gamma Oscillations. *Annu. Rev. Neurosci.* (2012). doi:10.1146/annurev-neuro-062111-150444

20. Buzsáki, G., Anastassiou, C. A. & Koch, C. The origin of extracellular fields and currents-EEG, ECoG, LFP and spikes. *Nature Reviews Neuroscience* (2012). doi:10.1038/nrn3241

21. Singer, W. Neuronal Synchrony: A Versatile Code for the Definition of Relations? *Neuron*

24, 49–65 (1999).

22. Yamamoto, J., Suh, J., Takeuchi, D. & Tonegawa, S. Successful Execution of Working Memory Linked to Synchronized High-Frequency Gamma Oscillations. *Cell* **157,** 845–857 (2014).

23. Arnulfo, G., Narizzano, M., Cardinale, F., Fato, M. M. & Palva, J. M. Automatic segmentation of deep intracerebral electrodes in computed tomography scans. *BMC Bioinformatics* (2015). doi:10.1186/s12859-015-0511-6

24. Thomas Yeo, B. T. *et al.* The organization of the human cerebral cortex estimated by intrinsic functional connectivity. *J. Neurophysiol.* **106,** 1125–1165 (2011).

25. Schaefer, A. *et al.* Local-Global Parcellation of the Human Cerebral Cortex from Intrinsic Functional Connectivity MRI. *Cereb. Cortex* (2017). doi:10.1093/cercor/bhx179

26. Raichle, M. E. *et al.* A default mode of brain function. *Natl. Acad. Sci.* **16;98(2),** 676–82 (2001).

27. Halgren, M. *et al.* Superficial Slow Rhythms Integrate Cortical Processing in Humans. *Sci. Rep.* (2018). doi:10.1038/s41598-018-20662-0

28. Monto, S., Palva, S., Voipio, J. & Palva, J. M. Very Slow EEG Fluctuations Predict the Dynamics of Stimulus Detection and Oscillation Amplitudes in Humans. *J. Neurosci.* (2008). doi:10.1523/JNEUROSCI.1910-08.2008

29. Vanhatalo, S. *et al.* Infraslow oscillations modulate excitability and interictal epileptic activity in the human cortex during sleep. *Proc. Natl. Acad. Sci.* (2004). doi:10.1073/pnas.0305375101

30. Nir, Y. *et al.* Coupling between Neuronal Firing Rate, Gamma LFP, and BOLD fMRI Is Related to Interneuronal Correlations. *Curr. Biol.* (2007). doi:10.1016/j.cub.2007.06.066

31. Mukamel, R. *et al.* Coupling Between Neuronal Firing, Field Potentials, and fMRI in Human Auditory Cortex. *Science (80-.).* **309,** 951 (2005).

32. Jacobs, J. *et al.* High-frequency electroencephalographic oscillations correlate with outcome of epilepsy surgery. *Ann. Neurol.* (2010). doi:10.1002/ana.21847

33. Vidal, J. R. *et al.* Long-Distance Amplitude Correlations in the High Gamma Band Reveal Segregation and Integration within the Reading Network. *J. Neurosci.* **32,** 6421–6434 (2012).

34. Khodagholy, D., Gelinas, J. N. & Buzsáki, G. Learning-enhanced coupling between ripple oscillations in association cortices and hippocampus. *Science (80-.).* (2017). doi:10.1126/science.aan6203

35. Tagliazucchi, E. & Laufs, H. Decoding Wakefulness Levels from Typical fMRI Resting-State Data Reveals Reliable Drifts between Wakefulness and Sleep. *Neuron* (2014). doi:10.1016/j.neuron.2014.03.020

36. Barttfeld, P. *et al.* Signature of consciousness in the dynamics of resting-state brain activity.

Proc. Natl. Acad. Sci. (2015). doi:10.1073/pnas.1418031112

37. Zhigalov, A. *et al.* Modular co-organization of functional connectivity and scale-free dynamics in the human brain. (2017). doi:10.1162/netn_a_00008

38. Vidaurre, D. *et al.* Spontaneous cortical activity transiently organises into frequency specific phase-coupling networks. *Nat. Commun.* **9,** (2018).

39. O'Neill, G. C. *et al.* Dynamics of large-scale electrophysiological networks: A technical review. *Neuroimage* **180,** 559–576 (2017).

40. Vidaurre, D., Smith, S. M. & Woolrich, M. W. Brain network dynamics are hierarchically organized in time. *Proc. Natl. Acad. Sci.* **114,** 201705120 (2017).

41. Otsubo, H. *et al.* High-frequency oscillations of ictal muscle activity and epileptogenic discharges on intracranial EEG in a temporal lobe epilepsy patient. *Clin. Neurophysiol.* (2008). doi:10.1016/j.clinph.2007.12.014

42. Palva, S. & Palva, J. M. Discovering oscillatory interaction networks with M/EEG: Challenges and breakthroughs. *Trends in Cognitive Sciences* (2012). doi:10.1016/j.tics.2012.02.004

43. Frauscher, B. *et al.* High-frequency oscillations: The state of clinical research. *Epilepsia* (2017). doi:10.1111/epi.13829

44. Brázdil, M. *et al.* Very high-frequency oscillations: Novel biomarkers of the epileptogenic zone. *Ann. Neurol.* (2017). doi:10.1002/ana.25006

45. Roehri, N. *et al.* High-frequency oscillations are not better biomarkers of epileptogenic tissues than spikes. *Ann. Neurol.* (2018). doi:10.1002/ana.25124

46. Jacobs, J. *et al.* Removing high-frequency oscillations. *Neurology* (2018). doi:10.1212/WNL.0000000000006158

47. Buzsáki, G. Hippocampal sharp wave-ripple: A cognitive biomarker for episodic memory and planning. *Hippocampus* **25,** 1073–1188 (2015).

48. Jefferys, J. G. R. *et al.* Mechanisms of physiological and epileptic HFO generation. *Progress in Neurobiology* (2012). doi:10.1016/j.pneurobio.2012.02.005

49. Shamas, M. *et al.* On the origin of epileptic High Frequency Oscillations observed on clinical electrodes. *Clin. Neurophysiol.* (2018). doi:10.1016/j.clinph.2018.01.062

50. Châtillon, C. E. *et al.* Influence of contact size on the detection of HFOs in human intracerebral EEG recordings. *Clin. Neurophysiol.* (2013). doi:10.1016/j.clinph.2013.02.113

Methods

Data acquisition

We recorded SEEG data from 67 subjects affected by drug resistant focal epilepsy and undergoing pre-surgical clinical assessment for the ablation of the epileptic focus. We acquired monopolar (with shared reference in the white matter far from the putative epileptic zone) local field potentials (LFPs) from brain tissue with platinum–iridium, multi-lead electrodes. Each penetrating shaft has 8 to 15 contacts, and the contacts were 2 mm long, 0.8 mm thick and had an inter-contact border-to-border distance of 1.5 mm (DIXI medical, Besancon, France). The anatomical positions and amounts of electrodes varied according to surgical requirements [1]. On average, each subject had 17 ± 3 (mean $\pm$ standard deviation) shafts (range 9-23) with a total of 153 ± 20 electrode contacts (range 122-184, left hemisphere: 66 ± 54, right hemisphere: 47 ± 55 contacts, grey-matter contacts: 110 ± 25). We acquired an average of 10 minutes of uninterrupted spontaneous activity with eyes closed in these patients with a 192-channel SEEG amplifier system (NIHON-KOHDEN NEUROFAX-110) at a sampling rate of 1 kHz. Before electrode implantation, the subjects gave written informed consent for participation in research studies and for publication of their data. This study was approved by the ethical committee (ID 939) of the Niguarda "Ca' Granda" Hospital, Milan, and was performed according to the Declaration of Helsinki.

Signal pre-processing

We excluded electrode contacts (1.3 ± 1.2, range 0–10, contacts) that demonstrate non-physiological activity from analyses. We employed a novel referencing scheme for SEEG data where electrodes in grey-matter were referenced by the contacts located in the closest white-matter (CW)[2]. This referencing scheme is proven optimal for preserving phase relationship between SEEG contact data[2]. Since one same white-matter contact can be used for referencing multiple cortical contacts, we rejected derivations with shared reference. The final size of channels analysed is on average 110 ± 25 for each subject and 7491 in total.

Prior to the main analysis, SEEG time series were filtered with 18 Finite Impulse Response (FIR) band pass filters with central frequency (F_c) ranging from 2.50 to 320Hz. We used a relative bandwidth approach for filter banks such that pass band (W_p) and band stop (W_s) were defined as $0.5\times F_c$ and $2\times F_c$, respectively. We excluded all 50 Hz line-noise harmonics using a band-stop equiripple FIR filter with 1 % of maximal band-pass ripples and 3 up to 8Hz width for the stop band parameters.

16

Epileptic events such as interictal spikes are characterized by high-amplitude fast temporal dynamics as well as by widespread spatial diffusion. Due to possible filtering artefacts around epileptic spikes and the resultant increase in synchrony, we discard periods of 500ms containing Interictal Epileptic Events (IIE). We defined such periods as the temporal windows where at least 10% of cortical contacts demonstrated abnormal concurrent sharp peaks in more than half of the 18 frequency bands. Such episodes were excluded from within- and cross-frequency synchrony analysis. To identify such periods, we divided the signal in multiple 500 ms non-overlapping windows and detected IIE events in amplitude envelops as the time point exceeding 5 times the standard deviation greater than the channel mean amplitude.

Defining the epileptic zones based on seizure activities in SEEG signals

The epileptogenic and seizure propagation zone were identified by clinical experts by visual analysis of the SEEG traces[1,3]. *Epileptogenic* areas are the hypothetical brain areas that are necessary and sufficient for the origin and early organization of the epileptic activities [4], from where contacts recording often show low voltage fast discharge or spike and wave events at seizure onset. Seizure *propagation* area are recruited during the seizure evolution, but they do not generate seizures [5,6], from where contact recording show delayed, rhythmic modifications after seizure initiation in the epileptogenic areas. In this study, we combined epileptogenic and propagation areas as the epileptogenic zone (EZ) to distinguish from the rest of brain areas that are referred to as *putative* healthy zones (nEZ).

Functional connectivity estimates

We estimated inter-areal phase-phase interactions at individual subject level using the Phase Locking Value (PLV). Defining $x'(t) = x(t) + iH[x(t)]$ as the analytical representation of the signal $x(t)$, where $H[\cdot\cdot]$ denotes the Hilbert transform, complex PLV (cPLV) is computed as [7]:

$$cPLV = \frac{1}{T}\sum_{t=1}^{T}\frac{x'(t)}{|x'(t)|}\frac{y'^{*}(t)}{|y'(t)|} \tag{1}$$

where T is length of the signal, and * indicates the complex conjugate. The PLV is the absolute value of complex cPLV ($PLV = |cPLV|$), and it is a scalar measure bounded between 0 and 1 indicating absence of phase and full phase synchronization, respectively.

Additionally, we used imaginary part of cPLV ($iPLV = Im(cPLV)$), metric insensitive to zero-lag interactions caused by volume conduction [8–10], for verification. For both PLV and iPLV connectivity, the fraction of significant edges (K) is the number of significant edges divided by the total possible edge number.

Statistical hypothesis tests

We estimated the null-hypothesis distributions of interaction metrics with surrogates that preserve the temporal autocorrelation structure of the original signals while abolishing correlations between two contacts. For each contact pair, we divided each contact's narrow band time series of into two blocks with a random time point k so that $x_1(t) = x(1 \dots k)$ and $x_2(t) = x(k \dots T)$, and constructed the surrogate as $x_{surr}(t) = [x_2, x_1]$. We computed surrogate PLV across all channel pairs and assembled the surrogate interaction matrix, and its means and standard deviations were later used in hypothesis testing.

Correlation estimates post-processing

To demonstrate the changes of interaction strength as a function of spatial distance between recording sites, we divided the inter-contact distances into three ranges (short (SH) 2 cm $\leq x < 4.6$ cm; medium (MD) 4.6 cm $\leq x < 6$ cm, and long-range (LG) $6 \leq x < 13$ cm) with same number of edges falling into each distance bin. Therefore, we averaged across subjects all the edges falling within each distance bin and for each frequency band separately (N=48702/range). The confidence intervals for PLV and iPLV, were expressed relatively to the surrogate means (SM) for PLV (3.42*SM corresponding to $p < 0.001$, Rayleigh distribution), and the surrogate standard deviations (SD) for iPLV (3.58*SD corresponding to $p < 0.001$, normal distribution).

To compare signals from superficial and deep layers in the grey matter (Fig. 4 and Suppl. Fig. 3), we divided the contacts into "shallow" and "deep" based their Grey Matter Proximity Index (GMPI)[2] that is defined as the relative distance between the contact location and the nearest white-grey surface, normalized by the grey matter thickness at that location:

$$GMPI = [(C - W) \cdot (P - W)]/|P - W| \qquad (2)$$

where P(x, y, z), W(x, y, z) and C(x, y, z) are the vertices on the pial, white-matter surface and contact coordinates in 3D individually reconstructed brain from MRI scan, respectively. Values 0< GMPI < 1 indicate that the contact midpoint is located in grey matter whereas a negative GMPI indicates that the contact midpoint is in the white matter.

We used -0.3<GMPI<0 and 0.5<GMPI<1.2 to classify deep and superficial layer contacts respectively. Next, PLV and iPLV estimates were averaged across subjects between deep-deep (DD) and superficial-superficial (SS) contact-pairs. We tested for between groups difference with a paired permutation test (100 random samples created by shuffling SS and DD labels within

subjects; threshold for significance corrected for multiple comparisons with Bonferroni $p < 0.05/N$, with N=18).

Anatomical co-localization of SEEG implant and Functional System characterization

To show that high-gamma phase coupling is associated with a common systems-level mechanism, we assessed the fraction of significance (K) between functional systems[11]. We extracted cortical parcels from pre-surgical T1 MRI 3D-FFE (used for surgical planning) using Freesurfer [12], and we used the new Schaefer parcellation [13] that favours functional networks topology over structural (gyral) topology [14]. The resulting cortical meshes were divided (with a range of resolutions from 100 to 1000 parcels) into seven functional systems: Visual, somato-motor (SM), Dorsal Attentional (DAN), Ventral Attentional (VAN), Limbic, Fronto-parietal (FP), and Default Mode Network (DMN). This atlas does not include subcortical regions and thus subcortical contacts were discarded from this analysis. We thus assigned each cortical contact to a cortical parcel that belongs to a functional system. We then computed the fraction of significant edges (K) between 7 functional systems.

Note that we initially conducted this analysis in the Destrieux 148-parcel atlas [14], but we re-analysed the whole dataset with the Schaefer atlas [13] after its release for both verifying the observations in the Destrieux atlas and for achieving optimal parcel-to-system morphing quality.

Cross-frequency coupling of slow rhythm phase and fast rhythm amplitude

Two signals of distinct rhythms are cross-frequency phase-amplitude coupled (PAC) if the phase of a slow neuronal oscillation modulates the amplitude fluctuations of the faster neuronal oscillations. PAC can be estimated using phase synchronization, Euler's formula, or examining whether the power of fast rhythms is non-uniformly distributed over low-frequency phase [15–19].

The rationale is that if the power fluctuations of fast rhythms are modulated by the phase of the slow oscillations, the fluctuations of these two time-series should be synchronized. In this study, we estimated PAC with the phase locking value (PLV) as:

$$PLV = \left| \frac{1}{N} \sum_{n=1}^{N} e^{i\left(\theta_{amp}(n) - \theta_{phase}(n)\right)} \right| \tag{3}$$

where $\theta_{amp}(n)$ is the phase time series of the power envelope of fast rhythm while $\theta_{phase}(n)$ is the narrow band phase time series of the slow rhythm. When there is a consistent relationship between these two time-series, the vector length of the mean phase differences (in the polar coordinate across all n samples) should be greater than zero, and a maximum value of 1 indicates perfect

coupling. The significance of PAC PLV value was determined in the same manner in individual subjects as we conducted for 1:1 phase synchrony described earlier.

Community structure analyses

For each frequency, we morphed individual contact-PLV values via the median operation, to a group-level inter-regional PLV matrix where regions are the Schaefer atlas parcels[13]. Due to low inter-hemispheric contact coverage (see Fig. 1c), we tried module detection only within hemispheres. To identify the modules while accounting for missing values, we used consensus clustering approaches[21] for each frequency separately. We first generated 5000 variants of the functional network wherein each missing PLV edge was replaced by a randomly selected existing PLV edge. We then applied Louvain algorithm[20] to detect modules in each of the 5000 variants. The range of the resolution parameter γ, which influences the number of communities identified, was set from 1 to 1.5 with 0.05 interval. The resolution parameter (γ) weights the importance of the null model against which the original network is compared:

$$Q(\gamma) = \frac{1}{2m} \sum_{i,j} \left[a_{i,j} - \gamma p_{i,j} \right] \delta(\sigma_i, \sigma_j) \tag{4}$$

where m is the total number of edges, $a_{i,j}$ is the edge in row i and column j, while $p_{i,j}$ is the probability of observing a connection in that position by chance, according to the null model used. $\delta(\sigma_i, \sigma_j)$ is 1 when node i and node j belong to same community, and 0 otherwise. Values of resolution parameter γ less than 1 produces a small number of large communities since the null model is down-weighed. On the other hand, values of γ larger than 1 produce a high number of small communities since the null model is up-weighted.

To assess the consensus in community assignments, across the 5000 variants we first generated an alternative matrix representation where parcel pairs were set either to 1 or 0 depending on whether those pairs of regions are in the same module or not, respectively. These 5000 representations contain information about the partition without arbitrary numbering of the communities, hence allowing for relating different partitions to each other. After generating representations, we then averaged these 5000 representations and fed into Louvain method (with the same γ value as for the original 5000 partitions), to obtain a consensus partition of the functional network.

Assessing statistical significance of modularity

Modular organisation can be observed at a range of spatial scales. To determine the spatial scales (indicated by resolution parameter γ) at which significant modular structure can be detected by the

employed algorithm, we first identified modules at γ values from 1 to 1.5 using an identical procedure as above. Here, we used 100 variants (rather than 5000) of the original connectome in the consensus clustering procedure for identifying modules with. For the identified modular structure at each γ value, the 'modularity' output parameter was obtained, *i.e.*, the extent to which network can be sub-divided into non-overlapping modules. To determine if this modularity value was statistically significant, we generated equivalent random networks of the original network, by randomly rewiring of the network. For a single run of the randomisation procedure, each of the 100 variants of the functional connectome were randomised in the same way, to ensure consistency of the randomisation within a single run. Modules were then identified for this ensemble of 100 equivalent random networks, for the gamma values between 1 and 1.5, and the corresponding modularity value was obtained. This procedure was repeated 100 times, to obtain a distribution of modularity values corresponding to equivalent random networks. For the entire set of gamma values, modularity from the original network was z-scored with respect to the distribution of modularity values for equivalent random networks. The γ values for which modular structure had a z-scored modularity value > 2 were marked as statistically significant. This procedure was performed for frequencies from 113 Hz to 320 Hz, and for two hemispheres separately.

Assessing reliability of identified modules for each brain region

We determined for a identified modular structure, the reliability with which each brain region can be assigned to its module. We generated a set of 100 functional connectomes for each HGA frequency band by bootstrapping across subjects. For $1 < γ < 1.5$, we identified modules for each of the bootstrapped connectomes, via consensus clustering with 100 repetitions. Then, for each brain region, we generated a vector indicating the set of regions in its same module (indicated by 1) and those regions in other modules (indicated by 0). This vector was compared to the corresponding vector from the modular structure of the original functional connectome. In particular, we estimated the sum of the number of regions that were correctly located in the same module and the number that was correctly located in other modules (compared to the original modular structure), as a function of the total number of regions (excluding own region). This was done for each of the 100 bootstrapped functional connectomes and gave a measure between 0 and 1, of the similarity of the modular structure between the original and bootstrapped network, for that region. Values close to 1 across the 100 bootstrapped networks indicated that the assignment of the region to its module in the original network, is reliable. To ascertain a statistically significant and reliable module assignment, we created a null-distribution by estimating the same measure when the vector indicating the modular structure of a region is resampled 100 times (without replacement). The

21

module affiliation of a region was then considered to be reliable if the mean 'reliability' of the region across the 100 bootstrapped networks was higher than the 95th percentile value of null distribution of the mean across-boostrapped null 'reliability' of the region. As mentioned above, this was done for gamma values between 1 and 1.5, for each of the HGA frequency bands, for left and right hemispheres separately. Further, the number of regions whose module assignment is reliable was considered to be statistically significant, if this number was higher than the expected number of regions for whose module assignment was reliable by chance, as assessed from the matrix of across-bootstrapped null 'reliability' values.

Comparing patterns of connectivity between Yeo systems during sleep and resting

The distance between matrices of functional connectivity between Yeo systems for 'resting' and 'sleep' was measured by their dissimilarity, *i.e.*, 1−correlation between the two matrices. To assess if this dissimilarity was statistically significant, we generated a null distribution of dissimilarity values between 1000 pairs of surrogate group-level Yeo-Yeo functional connectivity, which were generated after randomly mixing 'rest' and 'sleep' subject-level matrices. The original dissimilarity between 'rest' and 'sleep' was considered statistically significant if it was higher than the maximum dissimilarity value from the null distribution.

PLV in amplitude bins

To assess whether larger values of phase synchrony were correlated with higher amplitude values, we estimated instantaneous amplitude and phase profiles of the filtered time-series by means of Hilbert transform. We then normalised each amplitude time-course by its median and divided the normalized amplitude samples in quintiles. For each frequency, we built an amplitude-amplitude correlation matrix containing the instantaneous phase difference between channel pairs of each time-samples at that amplitude bins. We discarded amplitude samples larger than twice the amplitude median to remove effects of subthreshold spikes. We quantified the number of time-samples falling in each bin as a simple amplitude correlation measure. We hypothesized that that, if a given contact pair is amplitude correlated, the time-samples would not be randomly distributed over amplitude bins. Indeed, it will result in highly skewed distribution of time-samples towards larger amplitude bins. On the other hand, in the absence of real amplitude correlation that distribution would be undistinguishable from a uniform distribution. Hence, to test for a moment-to-moment amplitude correlation, we quantified the distance of the time-sample distribution from a uniform distribution for each amplitude-amplitude bin under the above null-hypotheses of no

22

correlation. To quantify whether phase consistency was correlated with moment-to-moment amplitude modulation, we quantified PLV in each amplitude-amplitude bin. The PLV is a measure sensitive to the sample number used[22], hence we quantified the minimum number of samples falling in each bin and then quantified PLV in amplitude bin with matched time-samples. Specifically, for each contact pair, we computed instantaneous phase difference across the entire time course. By grouping instantaneous amplitude samples falling in same bin, we averaged phase differences in each amplitude bin and later averaged this quantity across channel pairs and subjects.

Figure captions

Figure 1
Cohort size ensures significant coverage of cortical interactions

a Number of non-epileptic contacts per cortical regions (Schaefer et al. 2017, 100 parcels). **b** Number of contacts per functional system (Yeo et al. 2011): visual (VIS), sensori-motor (SM), dorsal attention (DAN), ventral attention (VAN), limbic (LIM), fronto-parietal (FP) and default mode (DEF) systems. **c** Cortical functional connectivity coverage of Schaefer parcellation: The percentage of left-hemispheric (blue), right-hemispheric (yellow) and inter-hemispheric (red) regions pairs that are connected by at least *x* edges. Inter-hemispheric coverage was low. **d** Number of contact pairs connecting each pair of functional systems.

Figure 2
High-Gamma Activity shows significant and robust long-range phase synchrony.

a Mean phase synchrony strength and spatial extent (**b**) estimated with PLV as a function of frequency and in short (2 to 4.6 cm, pink), medium (4.6-6 cm, blue), and long (6 to 13 cm, green) distance ranges. Dashed lines represent surrogate (N=100) data level for $p<0.001$. Shaded areas represent confidence limits (two-tail; $p<0.05$) for bootstrapped values (N=100). **c-f** Examples from two distinct subjects of long-range HGA phase synchrony with non-zero phase lag (**c**, **d**) and near-zero phase lag (**e**, **f**), and their temporal relation to fluctuations in slow rhythms; MFG (azure traces): medial frontal gyrus, IPS (red traces): intra-parietal sulcus.

Figure 3
Neuro-anatomical localization of High-Gamma synchronization

a Mean PLV across HGA frequencies (113-320 Hz) between Yeo functional systems, *i.e.*, visual (VIS), sensori-motor (SM), dorsal attention (DAN), ventral attention (VAN), limbic (LIM), fronto-

parietal (FP) and default mode (DEF) systems. **b** The fraction of significant (K) contact-wise PLV edges ($p<0.01$) between Yeo functional systems. **c** Five identified modules in 190 Hz PLV adjacency matrix (50 parcels in left hemisphere). The allocation of left (**d**) and right hemisphere (**g**) cortical regions to modules in 190 Hz PLV matrix for a range of the Louvain resolution parameters. Neuro-anatomical localization of cortical modules for left (**e**) and right hemisphere (**h**) at 190 Hz (resolution parameter=1.3). Regions for which modules can be identified reliably are shown in dark shades while regions for which module assignment is unreliable are shown in corresponding lighter shades of the same color. **f, i** demarcation of the Yeo functional systems. White lines represent region boundaries.

Figure 4

High-Gamma phase synchrony differs between cortical layers

a Mean synchrony strength (PLV between contacts) at short (2−4.6 cm, pink), medium (4.6−6 cm, blue), and long (6−13 cm, green) distance ranges shows distinct spectral profiles for contact pairs in deep cortical layers (-0.3 < GMPI ≤ 0; blue) and contact pairs in superficial cortical layers (0.5 < GMPI < 1; red). Dots represent the frequencies at which the difference between the superficial and deep contact was significantly (permutation test, N=100: $p < 0.05$, Bonferroni corrected along with 18 frequencies). The GMPI value represents the distance between contact and white-gray-matter border normalized by the cortical thickness. Inset: mean PLV of superficial and deep layer contact in the HGA frequency range. Shaded areas: the confidence intervals of 2.5% and 97.5% of bootstrapped population variance (100 bootstraps re-sampled with replacement); dashed lines represent confidence limit for $p< 0.001$ computed from 100 surrogates. **b** Mean fraction of significance K with $p<0.001$ computed from 100 surrogates.

Figure 5

Stronger High-Gamma phase synchrony is associated with maximal amplitude correlations between cortical sites

a High amplitude (normalized) samples between contact pairs is correlated with high phase consistency between these contact pairs. x and y axis represent the quintiles of normalized amplitude profiles of a pair of contact channel 1 and channel 2, respectively. Each element in the matrix is the mean of instantaneous PLV between all significant channel pairs ($p <0.001$ with 100 surrogates) as a function of their moment-to-moment normalized amplitudes. **b** Strength of moment-to-moment amplitude correlation. Distribution of instantaneous phase samples (light grey)

24

in each amplitude bin and its distance from uniform distribution (black) of samples (*i.e.*, null-hypothesis for the absence of moment-to-moment amplitude correlation).

Figure 6

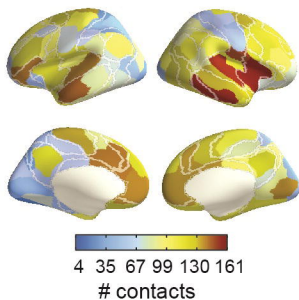**High-Gamma amplitude is modulated by the phase of slower oscillations a** Left: Among putatively healthy regions (nEZ), amplitude in higher frequencies (beta to low gamma) is coupled with the phase of low frequencies (theta to alpha). nPAC: population mean of individual phase-amplitude-coupling (PAC) PLV estimates normalized by within-subject surrogate mean. Right: fraction of significance *K* for phase-amplitude coupling on the population level. **b** Within the epileptogenic zone (EZ), prominent PAC is observed between delta, theta and alpha and faster brain rhythms. **c** Connections between EZ and nEZ recording sites also show PAC coupling between theta to alpha and faster brain rhythms.

Figure 7

Phase synchronization is stronger within the epileptogenic zone (EZ) in low frequencies

Top: At low frequencies (3-10Hz) and short-to-medium distances, mean phase synchrony among EZ regions (pink) is significantly stronger than for nEZ-nEZ (blue) or EZ-nEZ (green) connections. At higher frequencies (2nd to bottom row), this difference between EZ-EZ and nEZ-nEZ and EZ-nEZ recording site becomes insignificant across all distance ranges. Shaded areas represent 5th and 95th percentile of PLV values (bootstrapping, N=500). Distance ranges: short (2 cm $\leq x <$ 4.6 cm); medium (4.6 cm $\leq x <$ 6 cm), long (6 $\leq x <$ 13 cm)
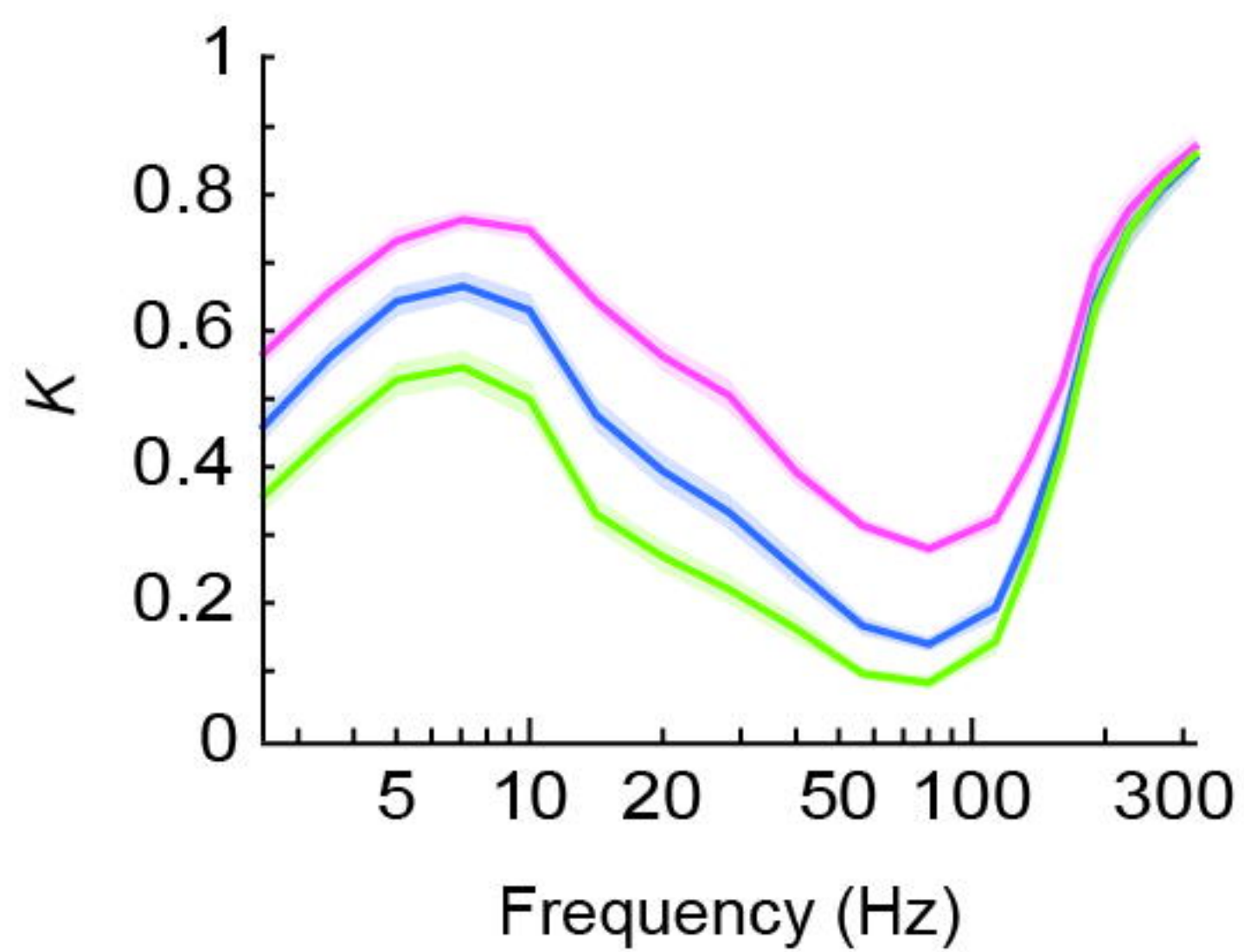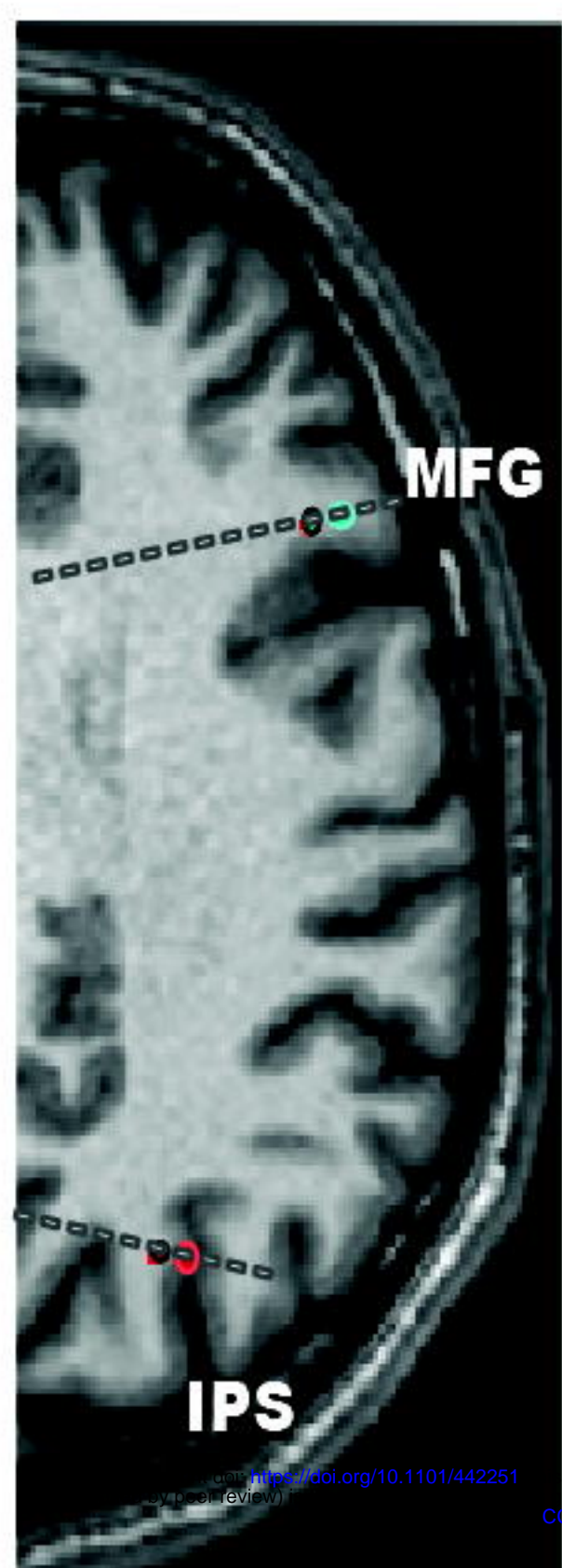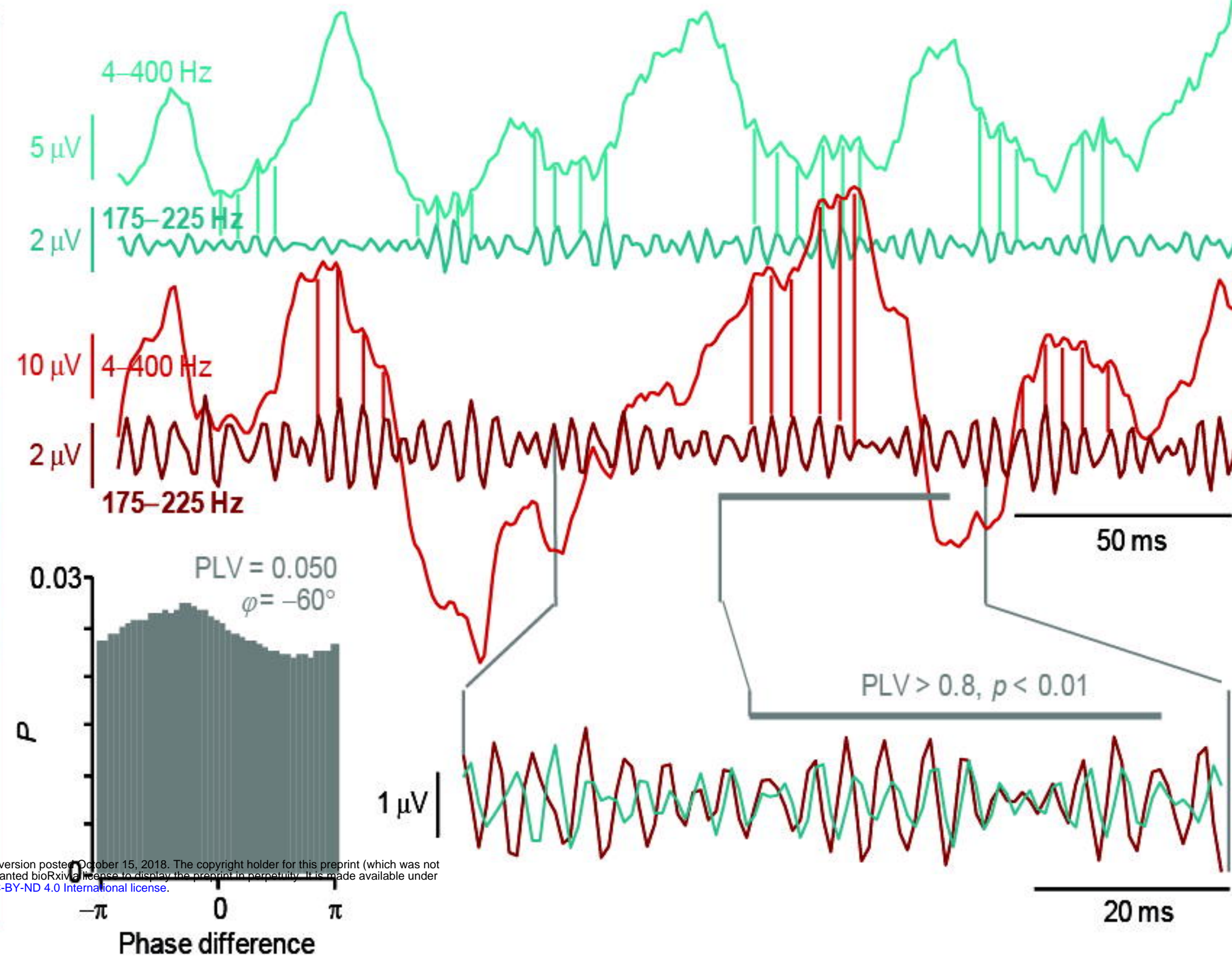
a Schaefer 100

b Yeo 7

4 35 67 99 130 161
contacts

182 422 662 902
contacts

c

coverage

— Left
— Right
— Inter

edges (x100)

d

DEF
FP
LIM
VAN
DAN
SM
VIS

VIS   DAN   LIM   DEF

25   125   224
edges (x100)

a

PLV

0.14
0.1
0.06
0.02

— Short
— Medium
— Long
--- Surrogate

5 10 20 50 100 300
Frequency (Hz)

b

K

1
0.8
0.6
0.4
0.2
0

5 10 20 50 100 300
Frequency (Hz)

c

MFG

IPS

d

4–400 Hz
5 µV
175–225 Hz
2 µV

10 µV 4–400 Hz
2 µV
175–225 Hz

50 ms

PLV = 0.050
$\varphi = -60°$
0.03
P
$-\pi$ 0 π
Phase difference

PLV > 0.8, $p < 0.01$

1 µV
20 ms

e

MFG

IPS

f

4–400 Hz
15 µV
225–275 Hz
2 µV

15 µV 4–400 Hz
2 µV
225–275 Hz

50 ms

PLV = 0.081
$\varphi = -1.1°$
0.03
P
$-\pi$ 0 π
Phase difference

PLV > 0.9, $p < 0.05$

1 µV
20 ms

a

Short | Medium | Long

PLV

Superficial
Deep
Surrogate

b

K

Frequency (Hz)

a nEZ-nEZ

b EZ-EZ

c nEZ-EZ

a